Suppression of errors in simulated ultrarelativistic bunch propagation using the *X*-dispersionless Maxwell solver

M. Filipovic,[*] C. Baumann,[†,‡] and A. Pukhov[§]

Institut für Theoretische Physik I, Heinrich-Heine-Universität Düsseldorf, 40225 Düsseldorf, Germany

(Received 17 September 2021; accepted 12 May 2022; published 31 May 2022)

Because of the inherent value of high-energy particle beams for the study of quantum electrodynamics effects, it is of great importance to accurately model the physics in numerical simulations. Numerical effects may alter the dynamics of a simulation and may change the physics of energy losses on account of the radiation reaction (RR) force. In this work, the numerical Cherenkov effect in combination with the RR force are analyzed in the vacuum propagation of an ultrarelativistic electron bunch. It is revisited that the use of the standard Yee solver in the present setup triggers the numerical Cherenkov instability. With the instability at hand, the simulation results of the Yee solver are compared to data obtained by the *X*-dispersionless Maxwell solver, also known as the rhombi-in-plane (RIP) solver. There, the numerical instability is suppressed by several orders of magnitude. Afterward, the impact of radiation reaction on the dynamics is studied for both cases. It is shown that the combination of the Yee solver and the RR force enhances the error significantly and the electron bunch loses about 90% of its energy as a result. These huge energy losses can be observed only if both the Lorentz force and the RR force are enabled in the code. In contrast, the RIP Maxwell solver is not plagued by these issues and accurately calculates the dynamics of the electron bunch.

DOI: 10.1103/PhysRevAccelBeams.25.054405

I. INTRODUCTION

High-energy charged particle beams are the key tools to study the very fundamental principles of physics. Experimentally, they can be used to test on the Standard Model [1], investigate the structure of matter [2], or synthesize exotic atomic nuclei [3]. Further research opportunities are expected due to the rapid progress in laser technology, where the realization of laser intensities above 10^{23} W cm^{-2} has been reported recently [4]. Therefore, large laser facilities such as ELI [5] or CoReLS (see also Refs. [6–8] for other facilities) will reach yet experimentally unexplored regimes of the light-matter interaction when combined with high-energy electrons. One of the major goals comprises deeper insights into radiation reaction (RR), a problem of electrodynamics that so far is not understood in all its details [9]. In addition, high-energy electrons might also be vital for studying the intensity frontier of quantum electrodynamics (QED) [10–13], where the theory is conjectured to become fully nonperturbative [14–16].

The key numerical platform to study interaction of (high-energy) charged particles with electromagnetic fields is the particle-in-cell (PIC) method. PIC simulations are considered to be the *ab initio* approach that covers a broad range of topics, from relativistic laser-plasma interactions [17–19] to plasma-based acceleration [20,21] and relativistic astrophysics [22,23]. In the PIC approach, matter is described as an ensemble of macroparticles, which are pushed according to the relativistic equations of motion. The resulting charge currents are used to update the electromagnetic fields, so allowing for a self-consistent description of the interaction [24]. The fields are commonly updated through finite-difference time-domain (FDTD) algorithms. Historically, Yee was one of the first who proposed a very successful staggered grid to solve the Maxwell equations in that way [25].

The Yee algorithm, however, is subject to numerical errors, which results in slowdown of the wave propagation velocity along all axes except (maybe) the grid diagonals. This is known as numerical dispersion and may trigger numerical instabilities, thus giving rise to nonphysical behavior. One prominent example is the numerical Cherenkov instability (NCI) in relativistic plasma simulations [26–28]. The instability is linked to the well-known Cherenkov radiation that is emitted when charges are faster than the electromagnetic phase velocity in the current

[*]marko.filipovic@hhu.de
[†]Present address: Institut für Energie- und Klimaforschung – Plasmaphysik, Forschungszentrum Jülich GmbH, 52425 Jülich, Germany.
[‡]christoph.baumann@tp1.hhu.de
[§]pukhov@tp1.hhu.de

medium. The numerical counterpart arises accordingly; i.e., when charged particles are faster than the numerical phase velocity, it comes to an unphysical coupling between electromagnetic modes and the particles. Physically, there should be no Cherenkov radiation in plasmas, because the phase velocity of electromagnetic modes in a background plasma is higher than the speed of light c. Unfortunately, simulations using the FDTD method—such as the Yee scheme—may show reduced phase velocities due to numerical dispersion. Therefore, NCI becomes visible once particle speed and phase velocity match.

NCI has been studied by several groups over the past years [29–35], and solutions to suppress it have already been proposed since its first observation. Different options how to achieve this are suggested in the literature like, for instance, the artificial increase of the speed of light in the field equations [27,36], the definition of a magnetic and electric field on the same spatial grid [27], the Galilean grid shift for a plasma flowing with uniform velocity [37], and other modification to the finite-difference time-domain algorithm [35]. Some other Maxwell solvers also achieved the suppression of nonphysical Cherenkov radiation from a relativistic beam [32,34]. Implementations of the latter methods are described in Refs. [30,38–42].

Apart from NCI, the Yee Maxwell solver can also lead to a phenomenon called numerical self-interaction. In that context, consider an ultrarelativistic high-current beam with Lorentz factor $\gamma_0 \gg 1$ and normalized velocity $\beta_\parallel \approx 1$ in vacuum. From the physics point of view, the electromagnetic self-field generated by such a beam is mainly transverse in the laboratory frame, and its electric and magnetic field are linked via the relation $B_\perp = \beta_\parallel E_\perp$ [43]. These beam fields cause an intrinsic force on a beam electron with charge $-e$ itself:

$$F_\perp = -e(E_\perp - \beta_\parallel B_\perp) = -e(E_\perp - \beta_\parallel^2 E_\perp) = -\frac{eE_\perp}{\gamma_0^2}, \quad (1)$$

which is negligible in the ultrarelativistic limit. It is also noted that relativistic electrons are subjected to a similar force when they are copropagating with a laser wave [44].

Unfortunately, the Yee scheme can overestimate the intrinsic self-force by orders of magnitude, which is a result from the staggered definition of electric and magnetic fields on the Yee lattice. As will be shown later, this causes dramatic energy losses of the high-current beam with time when the RR effect is taken into account. Such artifacts of induced radiation losses due to the numerically enhanced self-interaction are highly undesirable for many reasons. First, they hinder the analysis from numerical modeling of RR, as it might be unclear what causes specific energy losses. Second, they can strongly alter the dynamics of a system. This is especially unwanted when radiation losses have to be avoided (see, for instance, the discussion on the fully nonperturbative regime of QED in Refs. [10–13]). In other words, the Yee solver is not optimal for high-energy particle beams and should not be the first choice for an accurate modeling.

In this work, the aforementioned problems will be tackled through the semi-implicit X-dispersionless FDTD Maxwell solver initially developed for plasma-based acceleration [45]. The solver is dispersionless along the propagation direction, and the fields build rhombi-in-plane (RIP) patterns. Subsequently, the solver will be referred to as RIP solver throughout the manuscript. We study the vacuum propagation of a dense ultrarelativistic bunch, which carries extreme self-fields, so that QED effects can become relevant. The central problem here is to mitigate the numerical instability, which may hinder simulations of dense bunch vacuum propagation. The instability is due to the bunch self-interactions with its own fields resulting in huge radiation reaction forces as feedback. Mitigating this instability is crucial in the study of QED effects.

The paper is organized as follows. In Sec. II, the propagation of an ultrarelativistic electron bunch in vacuum is modeled with PIC simulations. The simulation will be performed with two independent Maxwell solvers, namely, the Yee and the RIP solver. NCI will be observed in the simulation performed with the Yee solver. Section II C summarizes the NCI under the two considered FDTD-based Maxwell solvers and explains the connection to the dispersion relation of the considered Maxwell solvers. Section III A describes the implementation of the RR force in the PIC code VLPL. Section III B reconsiders the previous simulations from Sec. II but now with enabled RR force. It will be discussed that the combination of the Yee solver and RR force is detrimental for the shown configuration and will lead to massive energy losses of the particles. Finally, Sec. IV draws a conclusion.

II. VACUUM BUNCH PROPAGATION WITH DIFFERENT MAXWELL SOLVERS

The propagation of an ultrarelativistic electron bunch in vacuum is considered via numerical simulations. The simulations are performed with two different solvers, namely, the Yee and the RIP solver. Please note that the simulations are first conducted without considering RR.

A. Simulation setup

The vacuum bunch propagation is simulated in the framework of full three-dimensional PIC simulations using the code VLPL [46,47]. This code can either use the Yee or the RIP [45] Maxwell solver to advance electromagnetic fields. All simulations utilize the moving window approach in a simulation box of dimension $20\sigma_0 \times 40\sigma_0 \times 40\sigma_0$ in the $X \times Y \times Z$ direction, where σ_0 represents the normalization of length. The transverse cell size is always set to $0.1\sigma_0 \times 0.1\sigma_0$. The longitudinal cell size, however, is different for the two Maxwell solvers. Along X, it is

$0.1\sigma_0$ for Yee and $0.05\sigma_0$ for RIP. The difference in the longitudinal step size results from the stability condition of the different solvers. The time step is $c\tau = 0.05\sigma_0$ in all simulations. The implemented electron bunch is configured as a spherical cloud with a Gaussian density profile $n_e = n_0 e^{-r^2/(4\sigma_r^2)}$, where n_0 and σ_r are the bunch's peak density and rms width, respectively. In these simulations, we use eight particles per cell. Furthermore, the electrons are propagating in the x direction with a momentum of $\mathbf{p}_0 = (p_{x0}, 0, 0)$. The boundaries of the simulation domain are absorbing for particles. At the beginning of the simulation, the fields on the grid generated by the electron bunch are initialized with a Poisson solver using as initial condition periodic boundaries. For the fields, the transverse boundaries are periodic, and the longitudinal ones are absorbing.

In particular, the specific simulation parameters are as follows: The peak density is $n_0 = 5n_c$ (here, $n_c = m_e c^2 \pi/(e^2\sigma_0^2)$ is the "normalized density"), the initial momentum is $p_{x0}/(m_e c) = 2.5 \times 10^5$ (m_e is the electron mass), and the radius parameter is $\sigma_r = \sigma_0 = 10$ nm (density in this configuration is normalized in a similar way as in laser plasma simulations, since VLPL is a relativistic PIC code for such applications and ties densities to the normalization of all lengths). Please note that the parameters are motivated by the electron bunch used in Ref. [11]. Such ultrarelativistic particle beams may radiate massively due to numerical self-action. For that reason, it is important to minimize numerical errors and to ascertain the origin of the radiation. This numerical instability can pose a limitation on the bunch length when simulating beam-beam collisions. Increasing the bunch length as an example in beam-beam collisions [11] increases the total simulation time where numerical errors can occur. In our simulations, the particles are not pushed until time $\approx 9T_b$, where T_b is the inverse of the relativistically corrected beam plasma frequency, $T_b = \omega_b^{-1} = \sqrt{\gamma_0 m_e/(4\pi e^2 n_0)}$. This time frame ensures that small nonphysical fields that might emerge due to the bunch initialization are cleared away and do not spoil the particle dynamics once momentum updates are applied. In this sense, the bunch propagates in self-consistent numerical grid fields, so that vacuum propagation can be simulated with higher accuracy for the case using the Yee solver. Subsequently, time $t = 0$ is measured relative to this time period.

B. Simulation results

Figure 1 presents data in the $x - y$ plane for the electron density and the transverse force obtained in simulations

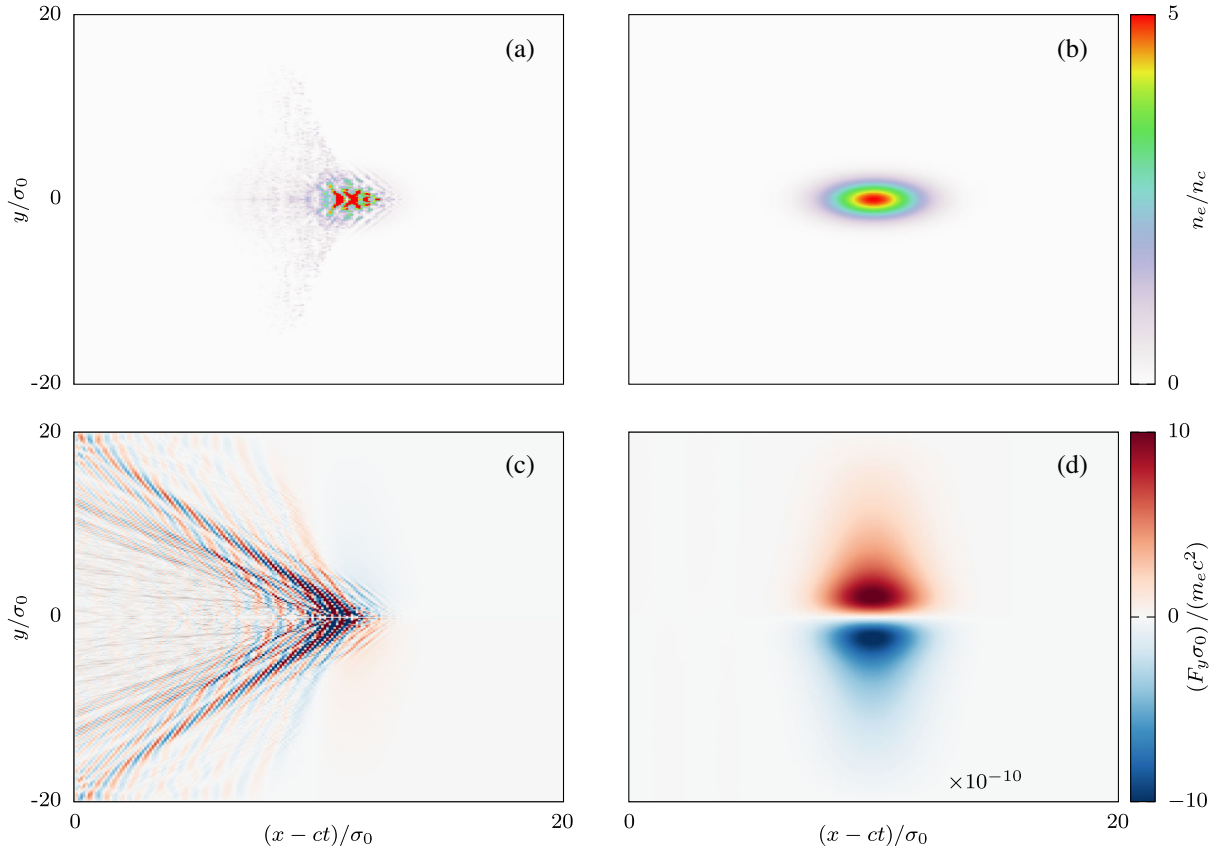

FIG. 1. Ultrarelativistic electron bunch propagating in vacuum without RR. Data for electron density [see (a) and (b)] and transverse force [see (c) and (d)] are shown at time $t/T_b = 10$. (a) and (c) show the results for the Yee solver, while (b) and (d) show the results for the RIP scheme. It is further noted that the data in (d) are scaled in order to apply the same color bar.

with the Yee solver [see Figs. 1(a) and 1(c)] and the RIP solver [see Figs. 1(b) and 1(d)]. After a simulation time of $t/T_b = 10$, the electron bunch is strongly deformed with the Yee solver [see Fig. 1(a)]. The bunch has been compressed, which increases the peak density to $18.3n_c$. In addition, the initial Gaussian density profile cannot be recognized anymore. The right-hand side of the bunch focuses, and the left-hand side smears out. Similar observations can be seen in the transverse force. We note here that we redefine the transverse force slightly with respect to Eq. (1). From now on, the transverse force is calculated from $F_y = E_y - B_z$, which has the advantage to be expressed solely by the fields and corresponds to ultrarelativistic particles moving with nearly the speed of light, $\beta = 1$. Figure 1(c) shows similar deformations also in the force. One can see waves at the rear that are too slow to comove with the bunch and form the Cherenkov cone. In addition, the force has built up significant amplitudes during the simulation. For instance, peak values of approximately $29m_ec^2/\sigma_0$ can be retrieved from the data which are definitely not negligible, so clearly indicating the onset of an instability.

The RIP solver in comparison does not create any visible numerical error during the simulation. The initial density profile is still preserved, which is expected for an ultrarelativistic electron bunch propagating in vacuum, as it experiences almost no self-interaction. The transverse force in this case is 10 orders of magnitude lower than in the simulation with the Yee scheme after the same simulation time. Moreover, the RIP simulation precisely reproduces the prediction for the self-force. Analytically, the self-force can be written along the y axis as $F_y(y) = -eE_y(y)/(2\gamma_0^2)$ [see the additional factor $1/2$ compared to Eq. (1) due to the redefinition of $F_\perp$]. Figure 2 shows the transverse force F_y

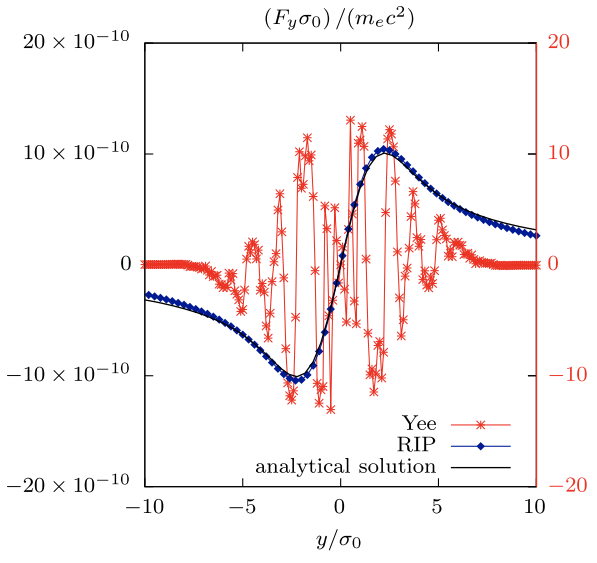

FIG. 2. Transverse force at $t/T_b = 10$ for a fixed x value of $(x - ct)/\sigma_0 = 10$. Transverse force obtained by the Yee solver uses the red y axis.

as a function of y at time $t/T_b = 10$ for a fixed x value of $(x - ct)/\sigma_0 = 10$. The analytical solution is in good agreement with the simulation data obtained by the RIP solver, whereas the data obtained by the Yee solver are ruined by numerical artifacts. Here, the faulty transverse force has been amplified and is 10 orders of magnitude bigger than the expected analytical solution. The transverse force obtained by the RIP solver shows a small discrepancy at large values of y ($|y| > 7.5\sigma_0$) in comparison to the analytical solution. This is due to the chosen periodic boundary conditions, which means that there is another electron bunch beyond the transverse boundaries. Their fields are directed such that they cancel the field of the main bunch at large coordinates, and, therefore, the transverse force decreases faster in the simulations than the analytical solution. This effect becomes less prominent if one increases the transverse size of the simulation domain. It can already be seen that the RIP solver yields a reduction of numerical errors.

C. Numerical Cherenkov instability in Maxwell solvers

To identify the observed numerical error in the configuration as NCI, a brief explanation is necessary to understand how the numerical approach gives rise to instabilities in the simulation. For that reason, it is important to take a look at the dispersion relation of the algorithms which are used to solve Maxwell equations.

The numerical instability appears if the dispersion relation of a numerical Maxwell solver allows electromagnetic modes which have a lower phase velocity v_{ph} than the speed of light c. Particles that travel close to c are now able to excite these modes and produce numerical Cherenkov radiation [37]. Therefore, it is likely that an ultrarelativistic electron bunch propagating in vacuum can excite such modes.

To determine the modes that are excited, it is first necessary to find the dispersion relations for the Maxwell solvers. This is usually done by inserting plane waves of the form

$$\mathbf{A} = \mathbf{A}_0 \exp\left(-i\omega t + i\mathbf{kr}\right) \tag{2}$$

into the numerical marching equations of the Maxwell solver (a detailed calculation can be found in Ref. [48]). The plane-wave analysis gives for the Yee solver

$$\frac{1}{h_x^2}\sin^2\left(\frac{k_x h_x}{2}\right) + \frac{1}{h_y^2}\sin^2\left(\frac{k_y h_y}{2}\right) + \frac{1}{h_z^2}\sin^2\left(\frac{k_z h_z}{2}\right) = \frac{1}{c^2\tau^2}\sin^2\left(\frac{\omega\tau}{2}\right) \tag{3}$$

and for the RIP solver in the special case of $c\tau = h_x$

$$\frac{1}{h_x^2}\sin^2\left(\frac{k_x h_x}{2}\right)+\left[1-\sin^2\left(\frac{k_x h_x}{2}\right)\right]\left[\frac{1}{h_y^2}\sin^2\left(\frac{k_y h_y}{2}\right)+\frac{1}{h_z^2}\sin^2\left(\frac{k_z h_z}{2}\right)\right]=\frac{1}{h_x^2}\sin^2\left(\frac{\omega h_x}{2c}\right). \tag{4}$$

The Yee dispersion relation suffers from v_{ph} different of c for all wave numbers except electromagnetic waves running along the grid diagonals, of $k_x = k_y$, $k_x = k_z$, or $k_y = k_z$ under the upper limit of the Courant-Friedrichs-Lewy (CFL) condition. The RIP solver is dispersionless for propagations along the x axis and exhibits similar properties in one-dimensional problems as the 1D advective solver by Birdsall and Langdon [24,45]. Both solvers store the transverse fields on the same integral positions and require the longitudinal grid step to be equal to the time step. These properties suppress nonphysical effects for $kh_x \sim \pm\pi$ [24]. Inserting $k_y = k_z = 0$ in the RIP dispersion relation [Eq. (4)], the equation reduces to $k_x = \omega/c$. For purely transverse wave numbers with $k_x = 0$, the RIP dispersion relation transforms to the 2D Yee dispersion relation [45]. One needs to be aware that just by plugging $k_y = k_z = 0$ into the Yee dispersion relation the Maxwell solver does not become dispersion-free. Stability of a Maxwell solver is, as above mentioned, also described by the CFL condition. The condition describes whether the used domain step sizes of the grid and the time step can guarantee that the propagation of fields is not faster than the phase velocity. The CFL condition of the Yee solver in a 3D space reads $c\tau < 1/\sqrt{(1/h_x)^2+(1/h_y)^2+(1/h_z)^2}$ [25,49]. The dispersionless property of the RIP solver should become advantageous for the considered configuration in this paper, since the electron bunch produces an electromagnetic field, which copropagates along the x axis.

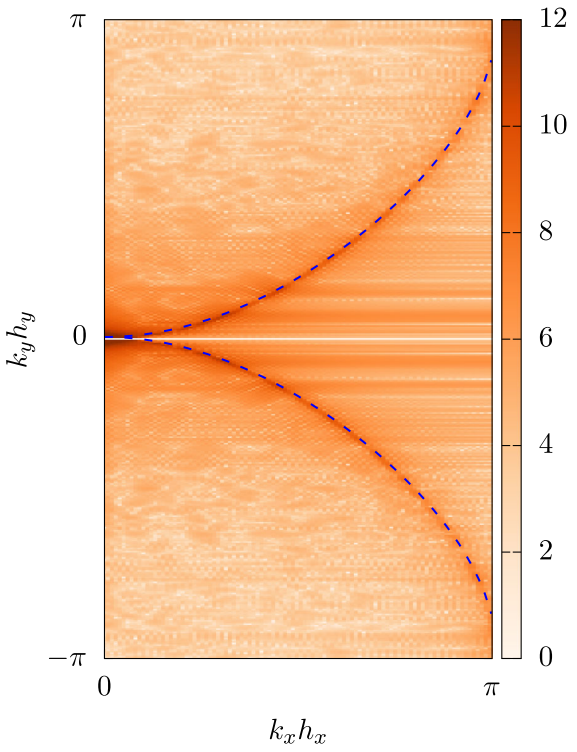

FIG. 3. Intensity of the spatial 2D FFT E_y component for $k_z = 0$ at time $t/T_b = 10$. The dashed line indicates the mode satisfying the dispersion relation for $v_{ph} = c$.

Linking the observed instability to the numerical Cherenkov instability can be confirmed the same way as performed by Lehe *et al.* in their study of the numerical Cherenkov effect [34]. Here, the solution of the Yee dispersion relation for excitable modes by NCI are calculated and compared the 2D FFT of the E_y component. Figure 3 displays the FFT of the component and highlighting the excitable mode with a dashed line similarly. This figure greatly coincides with the result in the work of Lehe *et al.* [34].

III. VACUUM BUNCH PROPAGATION WITH RADIATION REACTION

A. Radiation reaction force and its implementation in PIC codes

The simulations in the previous section discussed only the impact of the pure Lorentz force on the electron motion. However, if charged particles are subject to strong electromagnetic fields, they will emit high-frequency radiation. This, in turn, leads to a continuous loss of energy, which in classical electrodynamics is known under the term "radiation reaction" (RR). Physically, radiation reaction is mediated by an additional damping force acting on the charge. The most general form of radiation reaction is given the Lorentz-Abraham-Dirac (LAD) equation and has been proposed a long time ago [50]. Unfortunately, the model is plagued with physical inconsistencies such as preacceleration and runaway solutions, so that it is not the natural choice for an accurate numerical modeling. A vast number of approximated radiation reaction models can, therefore, be found in the literature, and all of them aim at circumventing the shortcomings of the LAD model (for instance, see [51] and the references therein). A similar approach is used in the present work. In particular, the damping force is calculated such that it dissipates the total emitted power as predicted by the relativistic Larmor formula [52]

$$P_{\mathrm{rad}} = \frac{2}{3}\alpha\frac{m^2c^4}{\hbar}\chi^2. \tag{5}$$

Here, $\alpha = e^2/(\hbar c) \simeq 1/137$ is the fine-structure constant, $\hbar$ is the reduced Planck constant, and

$$\chi = \frac{e\hbar}{m^2c^3}\sqrt{\left(\gamma\mathbf{E} + \frac{\mathbf{p}}{mc}\times\mathbf{B}\right)^2 - \left(\frac{\mathbf{p}}{mc}\cdot\mathbf{E}\right)^2} \quad (6)$$

measures the electric field in the particle's rest frame in units of the Schwinger field $m^2c^3/(e\hbar)$. For ultrarelativistic particles with Lorentz factors much larger than unity, $\gamma \gg 1$, one obtains

$$\mathbf{F}_{\mathrm{RR}} = -\frac{2}{3}\alpha\frac{mc^2}{\hbar}\chi^2 G(\chi)\frac{\mathbf{p}}{\gamma} \equiv -\nu_{\mathrm{RR}}\mathbf{p} \quad (7)$$

as the radiation reaction force, where the characteristic radiation loss frequency ν_{RR} is introduced. The factor $G(\chi)$ is known as the Gaunt factor and accounts for the fact that charges will emit less if χ approaches unity (i.e., when QED effects become important) [53,54]. In general, $G(\chi)$ is given by the complicated integral expression

$$G(\chi) = -\int_0^\infty \frac{3 + 1.25\chi s^{3/2} + 3\chi^2 s^3}{(1+\chi s^{3/2})^4}\mathrm{Ai}'(s)s\mathrm{d}s, \quad (8)$$

and its evaluation is computationally expensive. However, there is a fast and accurate approximation [55], which has been implemented into the PIC code VLPL:

$$G(\chi) \approx (1 + 18\chi + 69\chi^2 + 73\chi^3 + 5.806\chi^4)^{-1/3}. \quad (9)$$

Finally, the push due to RR is implemented directly after the Lorentz force push. Here, the damped momentum $\mathbf{p}_{\mathrm{RR}}$ is calculated as

$$\mathbf{p}_{\mathrm{RR}} = \frac{\mathbf{p}_L}{(1+\nu_{\mathrm{RR}}\tau)}, \quad (10)$$

where $\mathbf{p}_L$ is the momentum after the Lorentz force push.

B. Results of simulations with RR

In this section, the impact of RR on the vacuum bunch propagation of an ultrarelativistic electron bunch is studied for two Maxwell solvers. The other simulation parameters are unchanged with regard to the previous section. Figure 4 shows the results of the simulations with the additional force, again showing the density of the electron bunch [see Figs. 4(a) and 4(b)] and the transverse force F_y [see Figs. 4(c) and 4(d)]. Again, one can observe a disruption of the electron bunch when using the Yee solver [Fig. 4(a)]. This time the peak electron density is about $\approx 11.96 n_c$, which is lower in comparison to the case of the Yee solver without RR. This already indicates that RR further alters the bunch dynamics.

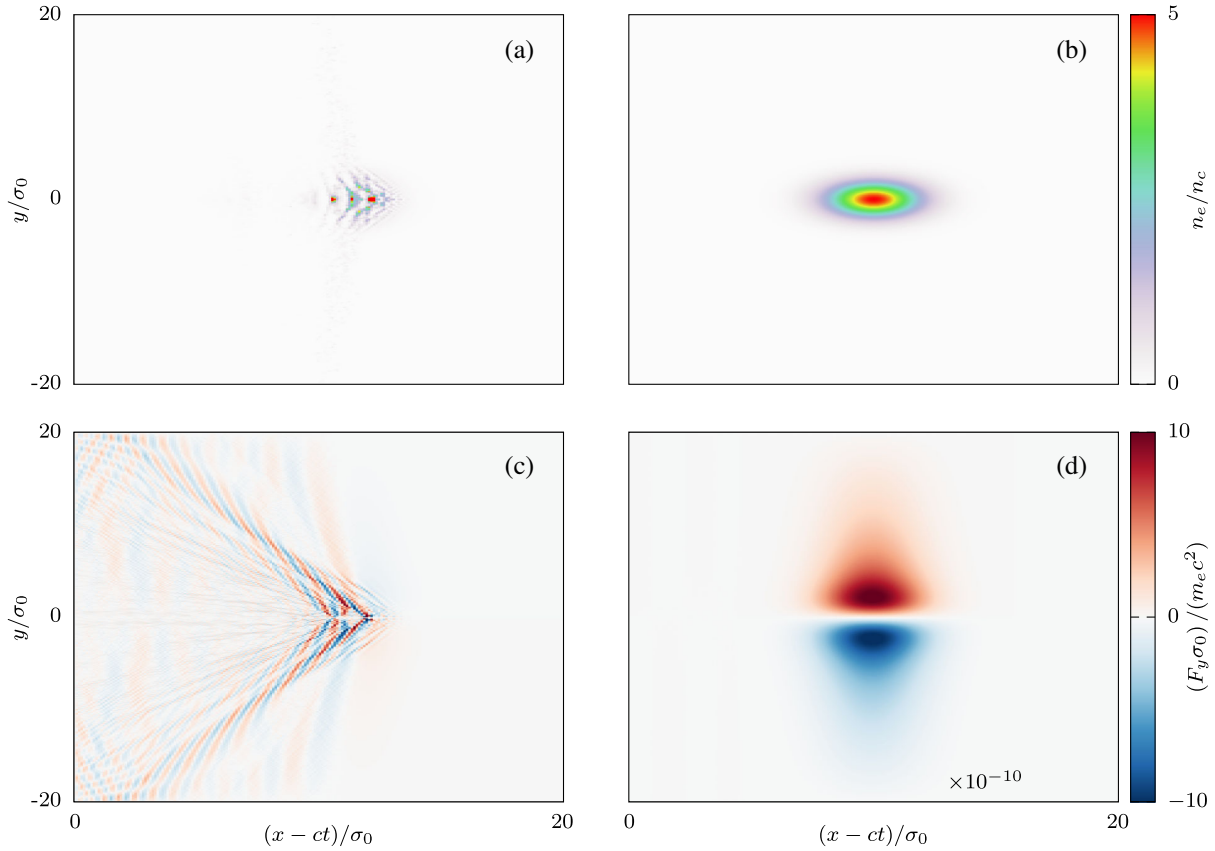

FIG. 4. Ultrarelativistic electron bunch propagating in vacuum with RR. The normalized electron density in n_e/n_c and the transverse force in dimensionless unit $(F_y\sigma_0)/(m_ec^2)$ are shown after $t/T_b = 10$. (a) and (c) show the data of the Yee solver and (b) and (d) the RIP solver. RR force is enabled in both simulations. The peak density of the data produced with the Yee solver increases to $n_e \approx 11.96 n_c$.

In contrast, the RIP solver once more does not show an instability and preserves the distribution of the electron bunch.

The maximum value of the transverse force is reduced in comparison to the simulation without RR [Fig. 4(c)], which is a result of the stronger electron bunch defocusing. One can see that the simulation performed with the RIP solver does not show these shortcomings, and the behavior of the electron bunch is similar to the previous simulation, so that it is not further influenced by enabling RR.

In principle, an ultrarelativistic bunch propagating purely along X should not be accompanied by a longitudinal magnetic field component B_x [43]. Therefore, the field energy associated with the longitudinal magnetic field component,

$$W_{B_x} = \frac{1}{8\pi}\int B_x^2 \mathrm{d}V, \tag{11}$$

can be used as a further tool to check for the validity of all simulations. Figure 5 presents the longitudinal magnetic field energy (11) as a log plot. The data show that both simulations with the RIP solver generate a negligible field, which is many orders of magnitudes below the level of the Yee simulations. Moreover, the RR does not impact the RIP simulations. On the contrary, one can immediately see that significant longitudinal magnetic fields are generated in the Yee simulations, which rise further within the simulation. In the beginning, the evolution of W_{B_x} shows a linear course in the log plot and is also independent of the RR force. After the distortion of the electron bunch, the linear trend changes and a second jump becomes apparent. In the following, one can observe that the evolution with and without RR splits up, and the simulation with enabled RR increases further to a certain value, after which it slowly decays. The data obtained without RR rise slower from that time, so that it looks like the instability is enhanced when the RR force is included.

We have seen that the RR leads to additional numerical artifacts in the vacuum propagation when using the Yee Maxwell solver. However, there is even another quantity that gets strongly affected and clearly shows nonphysical behavior. As the correct self-force is minuscule $[(F_\perp \sigma_0)/(m_e c^2) \sim 10^{-10}$ according to Eq. (1)], the characteristic radiation loss time ν_{RR}^{-1} is very long compared to the timescale T_b. Physically, this means that electrons should not suffer synchrotron radiation losses. Figure 6 depicts the simulation results for the energy ε of the electron bunch as a function of time (Yee and RIP solver with and without RR). In the simulation with RR and the Yee solver (blue curve), the particles are losing a significant amount of their initial energy ε_0 over time. The onset of the energy loss starts at time $t/T_b \approx 2$, which is also roughly the time at which the NCI begins. Afterward a major drop of the particle energy can be observed. Till the end of the simulation time, the energy of the electrons is reduced by ~91.4%. Such a dramatic drop in energy cannot be observed in any of the other simulations, so that it is not the result of the NCI alone.

In the other simulations, the particles are losing ~4.4% of their initial energy, and the energy loss scales linearly

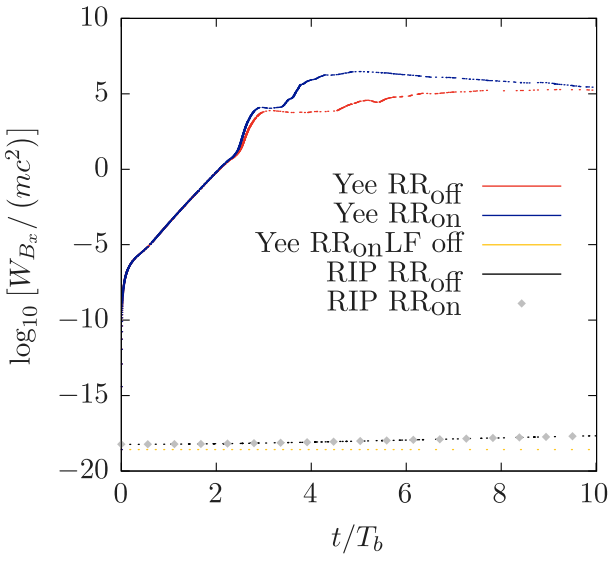

FIG. 5. Longitudinal magnetic field energy evolution for different Maxwell solvers and with or without accounting for RR. Additionally, the yellow line represents the simulation where the fields are updated with the Yee solver and the particles are solely pushed by the RR force; i.e., the momentum change by the Lorentz force (LF) has been ignored.

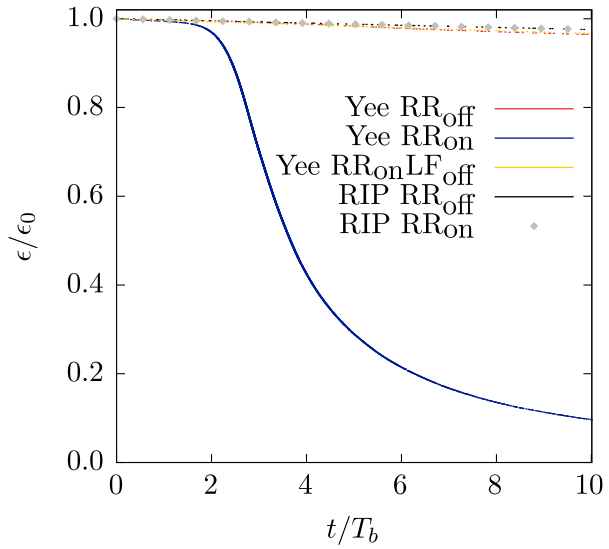

FIG. 6. Relative particle energy over time for an ultrarelativistic electron bunch propagating in vacuum. Additionally, the yellow line represents the simulation where the fields are updated with the Yee solver and the particles are solely pushed by the RR force; i.e., the momentum change by the LF has been ignored.

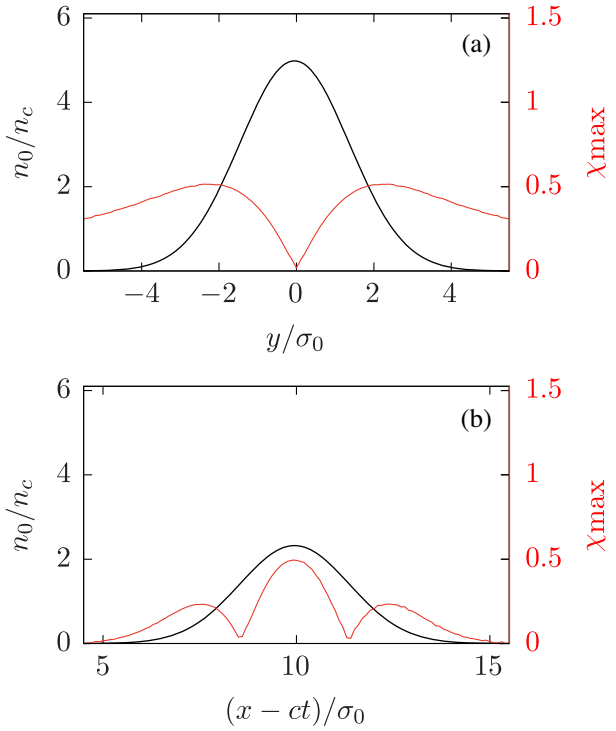

FIG. 7. The 3D PIC simulation result of an electron bunch propagating in a vacuum. Simulations have been performed with the Yee solver, activated radiation reaction force, and disabled Lorentz force at $t/T_b = 10$. (a) shows the electron density in critical densities and maximum quantum parameter within a cell for a fixed $(x-ct)/\sigma_0 = 20$ and $z/\sigma_0 = 0$. (b) shows electron density and $\chi_{\max}$ for a fixed $y/\sigma_0 = 1.8$ and $z/\sigma_0 = 0$, which slices the domain through the highest recorded quantum parameter value.

with time. This linear behavior comes from the nonvanishing field E_x, which is doing work of $-eE_xct$ on the bunch electrons. Thereby, the RIP simulation is in excellent agreement with the corresponding loss of energy when using the numerical data for E_x. The E_x field emerges in the PIC simulations because of the finite transverse size of the simulation box $L_\perp$ and scales as $E_x \sim L_\perp^{-2}$.

In a next step, it is of interest to confirm whether the rapid growth of the instability is due to the feedback loop between the emission of electromagnetic fields and their influence on the particle. To clarify the instability, an additional simulation has been performed with the same parameters but removed the Lorentz force from the particle pusher. Yet, we keep the radiation reaction force calculated on the electromagnetic fields at the particle position. In this regard, we suppress the feedback of emitted fields on the particle via Lorentz force.

The simulation data show that indeed the radiation of the electron bunch does not change significantly in this case. A relative energy loss of 5.82% at $t/T_b = 10$ has been recorded and can be seen in Fig. 6 (yellow curve). Therefore, the enabled RR force is not the primary factor causing the massive energy loss that has been observed earlier with all forces taken in consideration. Figure 7 shows the maximum quantum parameter in a cell with the electrons density overlapped at $t/T_b = 10$ with Fig. 7(a) showing the slice through the maximum electron density and Fig. 7(b) the slice through the maximum quantum parameter. Here, the electron bunch has not been deteriorated by the RR force alone. The reason for that lies within the quantum parameter, which is still low and higher values

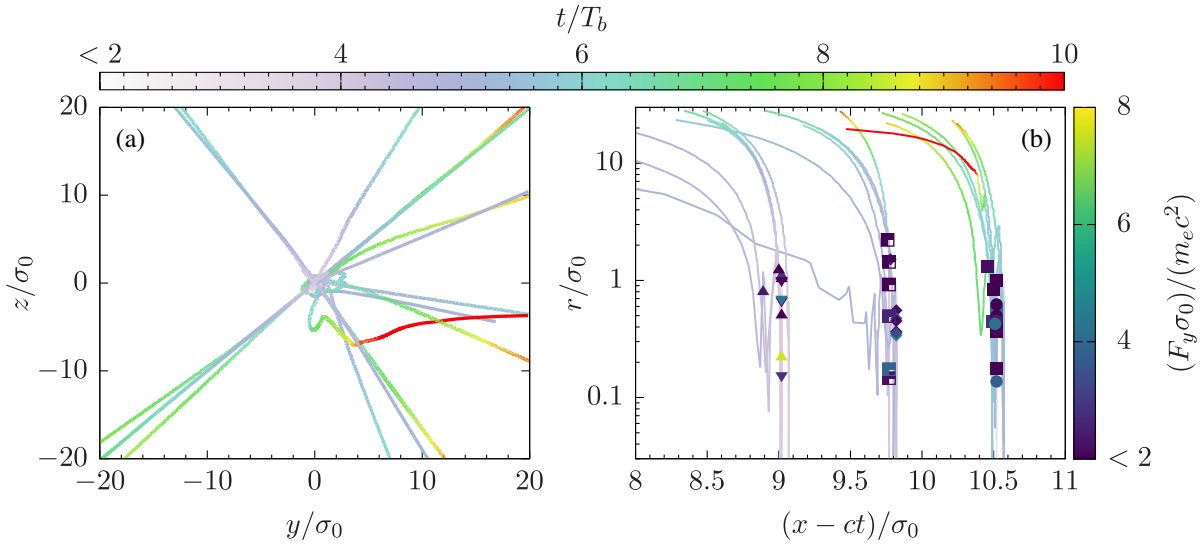

FIG. 8. The 3D PIC simulation result of an electron bunch propagating in a vacuum. Fields are calculated with the Yee solver and RR force is enabled. Here, 18 different particles have been tracked and the transverse force in their cell documented. (a) shows the particle displacement in the x and y direction. (b) shows the tracked particles in a $x-r-F_y$ plot. The trajectories are colored according to the simulation time. The points at certain times are color coded according to the transverse force within the cell, where the particle is currently located. Only transverse force values bigger than 2 have been displayed. Forces are displayed for two particles, respectively, at initial positions of $(x-ct)/\sigma_0 = 9.00$, $(x-ct)/\sigma_0 = 9.75$, and $(x-ct)/\sigma_0 = 10.50$.

can be found only at low electron density regions, as the maximum quantum parameter is not located in the center of the bunch. In contrast, the maximum quantum parameter rises to a value of 153.16 at $t/T_b \sim 2.68$ for the simulation with both the Yee mesh and the RR module used. This brings the electron bunch into a region where the QED effect would become likely and the RR force applies a strong dampening on the particles. Therefore, the Lorentz force is necessary to grow the feedback between the fields and the dynamics of the particles and characteristic for a numerical Cherenkov instability.

Finally, to advance the discussion of particle dynamics within the electron bunch, several particles have been tracked through the vacuum propagation computed with the Yee solver and taking the RR force in consideration. Particles which have been tracked were chosen at various positions within the electron density. The tracked particle results are summarized in Fig. 8. Figure 8(a) shows the trajectories of the tracked particle in the yz plane with the time being color coded. Once the instability takes place, particles are scattered to the edge. Figure 8(b) adds the transverse force F_y while showing the radial and longitudinal displacement. Particles start to deflect only radially first, since they are impacted by the transverse force. The first major transverse force influence occurs at $t \sim 2.5T_b$. Once the initial displacement takes place, all particles decelerate and fall behind, reducing their initial x position within the bunch. No strong transverse force can be seen at that point. After getting decelerated, the particles start to leave the moving simulation domain and are finally lost.

In summary, the data of energy loss show that the Yee solver may lead to completely wrong predictions. This, in turn, can have a major impact on the system dynamics.

IV. CONCLUSION

In this paper, the vacuum propagation of an ultrarelativistic electron bunch was studied in the framework of PIC simulations. Special focus was laid on the question of how the bunch dynamics will change if different Maxwell solvers are used. The standard Yee solver was shown to be plagued with NCI. As a result, the density profile of the ultrarelativistic electron bunch was significantly deformed over time. The addition of the RR effect in the simulation aggravates numerical problems of the Yee solver and leads to nonphysical energy losses. The bunch electrons lost about 90% of their initial energy.

In contrast, these numerical artifacts were absent when using the RIP Maxwell solver. This solver has the advantage to define electric and magnetic field at the same grid points and to be dispersion-free. The density profile of the electron bunch remained preserved over the entire simulation time. The incorporation of the RR force did not cause any numerical problems in this case. In particular, nonphysical radiation losses were not detected.

In conclusion, the RIP Maxwell solver showed very good results in the considered configuration and is a potential method to suppress the NCI as well as nonphysical radiation losses and, thus, is a very good choice for high-energy physics simulations. It makes it possible to study high-energy particle beams in quasi-1D problems for several periods like long bunch propagation, beam-beam collisions along one axis with high bunch lengths, and laser wake field acceleration.

ACKNOWLEDGMENTS

One of the authors (C. B.) is thankful for valuable discussions with Götz Lehmann. This work has been funded by the Deutsche Forschungsgemeinschaft (DFG) under Project No. 430078384. The authors gratefully acknowledge the Gauss Centre for Supercomputing e.V. ([56]) for funding this project (qed20) by providing computing time through the John von Neumann Institute for Computing (NIC) on the GCS Supercomputer JUWELS [57] at Jülich Supercomputing Centre (JSC). Computational infrastructure and support were also provided by the Centre for Information and Media Technology at Heinrich Heine University Düsseldorf.

APPENDIX: POISSON SOLVER WITH QUASISTATIC EQUATIONS

The initialization of the electromagnetic fields by a relativistic charge distribution ρ is determined by the quasistatic approximation. It is assumed that changes in our distribution are progressing slowly only over a distance of its own length. Therefore, all derivatives in dependence of the slow time τ are neglected, and fields are implemented for a specific time τ. After the initialization, the simulation proceeds with the time step entered for the simulation.

To derive the necessary quasistatic equations, we start with the Maxwell equations

$$\frac{\partial \mathbf{E}}{\partial t} = c\nabla \times \mathbf{B} - 4\pi \mathbf{j}, \tag{A1}$$

$$\frac{\partial \mathbf{B}}{\partial t} = -c\nabla \times \mathbf{E}, \tag{A2}$$

$$\nabla \cdot \mathbf{E} = 4\pi\rho, \tag{A3}$$

$$\nabla \cdot \mathbf{B} = 0 \tag{A4}$$

with $\mathbf{E}$ and $\mathbf{B}$ being the electric and magnetic fields, respectively, and $\mathbf{j}$ the current density generated by the propagation of the charges in the domain.

Applying the quasistatic approximation requires the introduction of new variables

$$\tau = t, \tag{A5}$$

$$\zeta = x - ct. \tag{A6}$$

In the next step, the Maxwell equations (A1)–(A4) are rewritten with the new variables (A5) and (A6):

$$c\nabla \times \mathbf{B} = -c\frac{\partial \mathbf{E}}{\partial \zeta} + 4\pi \mathbf{j}, \tag{A7}$$

$$c\frac{\partial \mathbf{B}}{\partial \zeta} = c\nabla \times \mathbf{E}, \tag{A8}$$

$$\nabla \cdot \mathbf{E} = 4\pi\rho, \tag{A9}$$

$$\nabla \cdot \mathbf{B} = 0. \tag{A10}$$

Here, all time derivatives are neglected, since

$$\frac{\partial}{\partial \tau} \ll \frac{\partial}{\partial \zeta}. \tag{A11}$$

Combining the curl of the rewritten Ampére law (A7) with the ζ derivative of the Faraday law (A8), the first quasistatic equation for the magnetic field,

$$\nabla_\perp^2 \mathbf{B} = -\frac{4\pi}{c}\nabla \times \mathbf{j}, \tag{A12}$$

is obtained. Please note that the $\nabla_\perp$ operator applies only on the directions transverse to propagation.

The second quasistatic equation regarding the electric field can be derived with the gradient of the Poisson law (A9) and the identity $\nabla(\nabla \cdot \mathbf{E}) = \nabla^2\mathbf{E} + \nabla \times \nabla \times \mathbf{E}$. The quasistatic equation for the transverse electric fields reads then

$$\nabla_\perp^2 \mathbf{E}_\perp = 4\pi\left(\nabla_\perp \rho - \frac{1}{c}\partial_\zeta \mathbf{j}_\perp\right). \tag{A13}$$

These equations allow the initialization of relativistic charge propagation in our code under the quasistatic approximation.

Further information about the implementation of quasistatic equations in VLPL can be found in Ref. [47].

[1] R. H. Parker, C. Yu, W. Zhong, B. Estey, and H. Müller, Measurement of the fine-structure constant as a test of the standard model, Science **360**, 191 (2018).

[2] A. Deshpande, R. Milner, R. Venugopalan, Vogelsang, and Werner, Study of the fundamental structure of matter with an electron-ion collider, Annu. Rev. Nucl. Part. Sci. **55**, 165 (2005).

[3] B. Franzke, H. Geissel, and G. Mnzenberg, Mass and lifetime measurements of exotic nuclei in storage rings, Mass Spectrom. Rev. **27**, 428 (2008).

[4] J. W. Yoon, Y. G. Kim, I. W. Choi, J. H. Sung, H. W. Lee, S. K. Lee, and C. H. Nam, Realization of laser intensity over 10^{23} w/cm^2, Optica **8**, 630 (2021).

[5] Whitebook ELI—Extreme Light Infrastructure: Science and Technology with Ultra-Intense Lasers, https://eli-laser.eu/media/1019/eli-whitebook.pdf.

[6] C. Hernandez-Gomez, S. Blake, O. Chekhlov, R. Clarke, A. Dunne, M. Galimberti, S. Hancock, R. Heathcote, P. Holligan, A. Lyachev *et al.*, The Vulcan 10 PW project, J. Phys. Conf. Ser. **244**, 032006 (2010).

[7] J. Zou, C. Le Blanc, D. Papadopoulos, G. Chériaux, P. Georges, G. Mennerat, F. Druon, L. Lecherbourg, A. Pellegrina, and P. Ramirez, Design and current progress of the Apollon 10 PW project, High Power Laser Sci. Eng. **3**, e2 (2015).

[8] C. N. Danson, C. Haefner, J. Bromage, T. Butcher, J.-C. F. Chanteloup, E. A. Chowdhury, A. Galvanauskas, L. A. Gizzi, J. Hein, D. I. Hillier *et al.*, Petawatt and exawatt class lasers worldwide, High Power Laser Sci. Eng. **7**, e54 (2019).

[9] T. G. Blackburn, Radiation reaction in electron-beam interactions with high-intensity lasers, Rev. Mod. Plasma Phys. **4**, 5 (2020).

[10] T. G. Blackburn, A. Ilderton, M. Marklund, and C. P. Ridgers, Reaching supercritical field strengths with intense lasers, New J. Phys. **21**, 053040 (2019).

[11] V. Yakimenko, S. Meuren, F. Del Gaudio, C. Baumann, A. Fedotov, F. Fiuza, T. Grismayer, M. J. Hogan, A. Pukhov, L. O. Silva *et al.*, Prospect of Studying Nonperturbative QED with Beam-Beam Collisions, Phys. Rev. Lett. **122**, 190404 (2019).

[12] C. Baumann, E. N. Nerush, A. Pukhov, and I. Y. Kostyukov, Probing non-perturbative QED with electron-laser collisions, Sci. Rep. **9**, 9407 (2019).

[13] C. Baumann and A. Pukhov, Laser-solid interaction and its potential for probing radiative corrections in strong-field quantum electrodynamics, Plasma Phys. Controlled Fusion **61**, 074010 (2019).

[14] V. Ritus, Radiative corrections in quantum electrodynamics with intense field and their analytical properties, Ann. Phys. (N.Y.) **69**, 555 (1972).

[15] N. B. Narozhny, Expansion parameter of perturbation theory in intense-field quantum electrodynamics, Phys. Rev. D **21**, 1176 (1980).

[16] A. Fedotov, Conjecture of perturbative QED breakdown at $\alpha\chi 2/3 \gtrsim 1$, J. Phys. Conf. Ser. **826**, 012027 (2017).

[17] I. Kostyukov, A. Pukhov, and S. Kiselev, Phenomenological theory of laser-plasma interaction in bubble regime, Phys. Plasmas **11**, 5256 (2004).

[18] A. Rousse, K. T. Phuoc, R. Shah, A. Pukhov, E. Lefebvre, V. Malka, S. Kiselev, F. Burgy, J.-P. Rousseau, D. Umstadter, and D. Hulin, Production of a keV X-Ray Beam from Synchrotron Radiation in Relativistic Laser-Plasma Interaction, Phys. Rev. Lett. **93**, 135005 (2004).

[19] A. Pukhov and J. Meyer-ter Vehn, Relativistic laser-plasma interaction by multi-dimensional particle-in-cell simulations, Phys. Plasmas **5**, 1880 (1998).

[20] J. Faure, Y. Glinec, A. Pukhov, S. Kiselev, S. Gordienko, E. Lefebvre, J.-P. Rousseau, F. Burgy, and V. Malka,

A laser-plasma accelerator producing monoenergetic electron beams, Nature (London) **431**, 541 (2004).
[21] S. F. Martins, R. Fonseca, W. Lu, W. B. Mori, and L. Silva, Exploring laser-wakefield-accelerator regimes for near-term lasers using particle-in-cell simulation in lorentz-boosted frames, Nat. Phys. **6**, 311 (2010).
[22] B. Cerutti and A. M. Beloborodov, Electrodynamics of pulsar magnetospheres, Space Sci. Rev. **207**, 111 (2017).
[23] A. A. Philippov and A. Spitkovsky, *Ab initio* pulsar magnetosphere: Three-dimensional particle-in-cell simulations of axisymmetric pulsars, Astrophys. J. Lett. **785**, L33 (2014).
[24] C. K. Birdsall and A. B. Langdon, *Plasma Physics via Computer Simulation* (CRC Press, Boca Raton, 1991).
[25] K. Yee, Numerical solution of initial boundary value problems involving Maxwell's equations in isotropic media, IEEE Trans. Antennas Propag. **14**, 302 (1966).
[26] B. B. Godfrey, Canonical momenta and numerical instabilities in particle codes, J. Comput. Phys. **19**, 58 (1975).
[27] B. B. Godfrey, Numerical Cherenkov instabilities in electromagnetic particle codes, J. Comput. Phys. **15**, 504 (1974).
[28] J. P. Boris and R. Lee, Nonphysical self forces in some electromagnetic plasma-simulation algorithms, J. Comput. Phys. **12**, 131 (1973).
[29] D.-Y. Na, J. L. Nicolini, R. Lee, B.-H. Borges, Y. A. Omelchenko, and F. L. Teixeira, Diagnosing numerical Cherenkov instabilities in relativistic plasma simulations based on general meshes, J. Comput. Phys. **402**, 108880 (2020).
[30] B. B. Godfrey, Review and recent advances in PIC modeling of relativistic beams and plasmas, AIP Conf. Proc. **1777**, 020004 (2016).
[31] X. Xu, P. Yu, S. F. Martins, F. S. Tsung, V. K. Decyk, J. Vieira, R. A. Fonseca, W. Lu, L. O. Silva, and W. B. Mori, Numerical instability due to relativistic plasma drift in EM-PIC simulations, Comput. Phys. Commun. **184**, 2503 (2013).
[32] X. Xu, F. Li, F. S. Tsung, T. N. Dalichaouch, W. An, H. Wen, V. K. Decyk, R. A. Fonseca, M. J. Hogan, and W. B. Mori, On numerical errors to the fields surrounding a relativistically moving particle in PIC codes, J. Comput. Phys. **413**, 109451 (2020).
[33] S. Jalas, I. Dornmair, R. Lehe, H. Vincenti, J.-L. Vay, M. Kirchen, and A. R. Maier, Accurate modeling of plasma acceleration with arbitrary order pseudo-spectral particle-in-cell methods, Phys. Plasmas **24**, 033115 (2017).
[34] R. Lehe, A. Lifschitz, C. Thaury, V. Malka, and X. Davoine, Numerical growth of emittance in simulations of laser-wakefield acceleration, Phys. Rev. Accel. Beams **16**, 021301 (2013).
[35] B. M. Cowan, D. L. Bruhwiler, J. R. Cary, E. Cormier-Michel, and C. G. R. Geddes, Generalized algorithm for control of numerical dispersion in explicit time-domain electromagnetic simulations, Phys. Rev. Accel. Beams **16**, 041303 (2013).
[36] R. Nuter and V. Tikhonchuk, Suppressing the numerical Cherenkov radiation in the Yee numerical scheme, J. Comput. Phys. **305**, 664 (2016).
[37] R. Lehe, M. Kirchen, B. B. Godfrey, A. R. Maier, and J.-L. Vay, Elimination of numerical Cherenkov instability in flowing-plasma particle-in-cell simulations by using Galilean coordinates, Phys. Rev. E **94**, 053305 (2016).
[38] F. Li, P. Yu, X. Xu, F. Fiuza, V. K. Decyk, T. Dalichaouch, A. Davidson, A. Tableman, W. An, F. S. Tsung *et al.*, Controlling the numerical Cerenkov instability in PIC simulations using a customized finite difference Maxwell solver and a local FFT based current correction, Comput. Phys. Commun. **214**, 6 (2017).
[39] B. B. Godfrey and J.-L. Vay, Suppressing the numerical Cherenkov instability in FDTD PIC codes, J. Comput. Phys. **267**, 1 (2014).
[40] J.-L. Vay, C. Geddes, E. Cormier-Michel, and D. Grote, Numerical methods for instability mitigation in the modeling of laser wakefield accelerators in a Lorentz-boosted frame, J. Comput. Phys. **230**, 5908 (2011).
[41] P. Yu, X. Xu, V. K. Decyk, F. Fiuza, J. Vieira, F. S. Tsung, R. A. Fonseca, W. Lu, L. O. Silva, and W. B. Mori, Elimination of the numerical Cerenkov instability for spectral EM-PIC codes, Comput. Phys. Commun. **192**, 32 (2015).
[42] P. Yu, X. Xu, A. Tableman, V. K. Decyk, F. S. Tsung, F. Fiuza, A. Davidson, J. Vieira, R. A. Fonseca, W. Lu, L. O. Silva, and W. B. Mori, Mitigation of numerical Cerenkov radiation and instability using a hybrid finite difference-FFT Maxwell solver and a local charge conserving current deposit, Comput. Phys. Commun. **197**, 144 (2015).
[43] F. Del Gaudio, T. Grismayer, R. A. Fonseca, W. B. Mori, and L. O. Silva, Bright γ rays source and nonlinear Breit-Wheeler pairs in the collision of high density particle beams, Phys. Rev. Accel. Beams **22**, 023402 (2019).
[44] R. Lehe, C. Thaury, E. Guillaume, A. Lifschitz, and V. Malka, Laser-plasma lens for laser-wakefield accelerators, Phys. Rev. Accel. Beams **17**, 121301 (2014).
[45] A. Pukhov, X-dispersionless Maxwell solver for plasma-based particle acceleration, J. Comput. Phys. **418**, 109622 (2020).
[46] A. Pukhov, Three-dimensional electromagnetic relativistic particle-in-cell code VLPL (virtual laser plasma lab), J. Plasma Phys. **61**, 425 (1999).
[47] A. Pukhov, Particle-in-cell codes for plasma-based particle acceleration, CERN Yellow Rep. **1**, 181 (2016).
[48] A. Taflove, S. C. Hagness, and M. Piket-May, Computational electromagnetics: The finite-difference time-domain method, in *The Electrical Engineering Handbook* (2005), Vol. 3, 10.1016/B978-012170960-0/50046-3.
[49] A. Blinne, D. Schinkel, S. Kuschel, N. Elkina, S. G. Rykovanov, and M. Zepf, A systematic approach to numerical dispersion in Maxwell solvers, Comput. Phys. Commun. **224**, 273 (2018).
[50] P. A. M. Dirac, Classical theory of radiating electrons, Proc. R. Soc. A **167**, 148 (1938).
[51] M. Vranic, J. Martins, R. Fonseca, and L. Silva, Classical radiation reaction in particle-in-cell simulations, Comput. Phys. Commun. **204**, 141 (2016).
[52] L. D. Landau and E. M. Lifshitz, *The Classical Theory of Fields* (Pergamon, Amsterdam, 1975).

[53] V. N. Baier, V. M. Katkov, and V. M. Strakhovenko, *Electromagnetic Processes at High Energies in Oriented Single Crystals* (World Scientific, Singapore, 1998).
[54] T. G. Blackburn, C. P. Ridgers, J. G. Kirk, and A. R. Bell, Quantum Radiation Reaction in Laser-Electron-Beam Collisions, Phys. Rev. Lett. **112**, 015001 (2014).
[55] T. Z. Esirkepov, S. S. Bulanov, J. K. Koga, M. Kando, K. Kondo, N. N. Rosanov, G. Korn, and S. V. Bulanov, Attractors and chaos of electron dynamics in electromagnetic standing waves, Phys. Lett. A **379**, 2044 (2015).
[56] www.gauss-centre.eu
[57] Jülich Supercomputing Centre, JUWELS cluster and booster: Exascale pathfinder with modular supercomputing architecture at Jülich Supercomputing Centre, J. Large-Scale Res. Facil. **7**, A183 (2021).